

# Quantum phase transitions in two dimensions: Experiments in Josephson-junction arrays

H. S. J. van der Zant, W. J. Elion, L. J. Geerligs, and J. E. Mooij

*Department of Applied Physics and Delft Institute of Microelectronics and Submicron-technology (DIMES),  
Delft University of Technology Lorentzweg 1, 2628 CJ Delft, The Netherlands*

(Received 21 May 1996)

We have studied two-dimensional superconducting networks coupled by Josephson junctions in the regime where the Josephson coupling energy is comparable in magnitude to the capacitive energy of charging an island with a Cooper pair. We have mapped out the dependence of quantum phase transitions on the ratio of these two energies (for different values of the applied magnetic field) and on the applied field for arrays both with square and triangular cells. Our experimental results are compared with existing theoretical predictions. [S0163-1829(96)07737-5]

## I. INTRODUCTION

In superconducting two-dimensional (2D) systems such as Josephson-junction arrays<sup>1</sup> and thin films<sup>2,3</sup> the localization of charge carriers and the corresponding enhancement of quantum-mechanical fluctuations of the phase of the superconductor order parameter induces superconductor-to-insulator (S-I) phase transitions. At the superconducting side of the transition, dynamics is determined by vortices whereas at the insulating side dynamics is determined by  $2e$  charge excitations. Near the S-I transition, vortex and charge dynamics compete. Here, vortices and charges must be viewed as bosonic quantum particles with long-range interactions. Artificially fabricated networks of superconducting islands weakly coupled by tunnel junctions are model systems for the study of these interacting bosons. Damping can be made small; control parameters can be measured and to a large extent be varied independently. Quantum interference of vortices<sup>4</sup> has been observed in a hexagon-shaped Josephson array and the existence of quantum Hall states in Josephson arrays has been predicted.<sup>5</sup>

At low temperatures there are two competing energy scales in Josephson arrays; the Josephson coupling energy  $E_J$ , the energy scale for the superconducting coupling between islands that permits transport of Cooper pairs and the charging energy  $E_C$ , the energy scale that tends to localize charge carriers. When  $E_J$  is much larger than  $E_C$ , the number of Cooper pairs on the islands is undetermined but the phase on the islands is well defined. In this regime, the classical motion of vortices determines the array dynamics. At low temperatures vortices are pinned in the intrinsic lattice potential and the arrays are superconducting. In the opposite limit  $E_C \gg E_J$ , the phase is undetermined so that vortices are subject to strong quantum fluctuations and the Coulomb blockade pins Cooper pairs to the islands; at low temperatures arrays are insulating. This superconducting-to-insulating (S-I) transition<sup>6-8</sup> induced by the charging energy is shown in Fig. 1(a), where three current-voltage ( $I$ - $V$ ) curves are plotted of three different samples of increasing  $E_C/E_J$  ratio.

A second control parameter that can be used to induce quantum phase transitions is the magnetic field,<sup>9</sup> which in arrays is denoted with the index  $f$ , the applied flux per cell divided by the flux quantum  $\Phi_0 = h/2e$ . In Fig. 1(b),  $I$ - $V$

characteristics of one sample are shown for three different values of the applied magnetic field. For this sample, a field of 1 G was used to drive the array from the superconducting state with a small critical current to the insulating state with a small Coulomb gap. Field-tuned S-I transitions occur in arrays with  $E_C \approx E_J$ ,<sup>10,11</sup> where quantum fluctuations are strong. This field-tuned transition can be explained in terms of a Bose-condensation of vortices.<sup>12</sup> With increasing magnetic field, the number of vortices increases and above a certain critical field Bose condensation occurs. The vortex superfluid leads to insulating behavior.

The duality between vortices and charges in Josephson arrays near the S-I transition<sup>13-16</sup> is clearly illustrated by Fig. 1. At the superconducting side of the transition, vortices

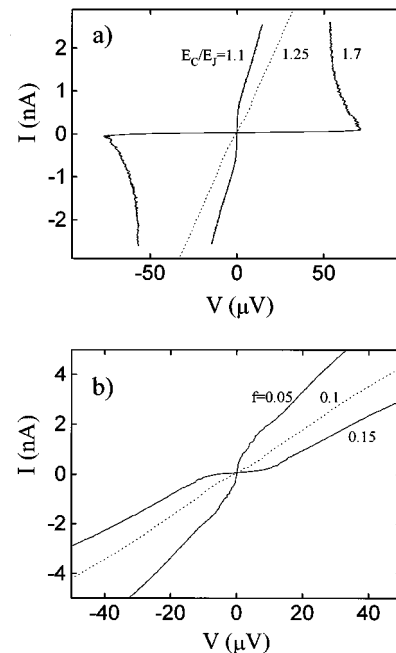


FIG. 1. Current-voltage characteristics measured at low temperatures as a function of (a) the ratio  $E_C/E_J$  and (b) the applied magnetic field (of a sample with  $E_C/E_J = 1.25$ ), showing the cross-over from superconducting behavior with a critical current to insulating behavior with a charging gap. The curve in (a) taken at  $E_C/E_J = 1.7$  has been scaled with a factor of  $1/8$  in the  $y$  axis.

remain pinned until the bias current exceeds a critical value above which superconductivity is destroyed by the motion of vortices. At the insulating side, charges are localized by the Coulomb blockade until the bias voltage exceeds a certain threshold value. Above the threshold voltage, charges are able to move and a conductance can be measured across the array.<sup>17–19</sup> This vortex-charge duality goes even further. Just as in the classical regime additional vortices can be induced by a magnetic field, in the insulating regime additional Cooper pairs can be brought onto the islands by applying a voltage between the ground potential and the array. The resulting uniform charge distribution is known as charge frustration and a charge-tuned S–I transition has been predicted theoretically.<sup>20</sup>

In this paper, we present an overview of the quantum phase transitions that occur in Josephson-junction arrays and we compare our experimental results with existing theories. The paper is organized as follows. In the next section, we summarize some of the basics of Josephson-junction arrays and comment on the similarities and differences with thin films. In Sec. III we discuss the array characteristics and the experimental details. Section IV summarizes the experimental results on the S–I transitions as a function of the  $E_C/E_J$  ratio in zero and commensurate magnetic fields. Section V deals with the field-tuned S–I transitions and the determination of its critical exponents. We briefly comment on the competing dynamics of vortices and charges near the S–I transition and show that the bias current/voltage can be viewed as a fourth (next to the  $E_C/E_J$  ratio, the magnetic field, and charge frustration) parameter to induce a S–I transition. In Sec. VI, our results of the S–I transitions as a function of  $E_C/E_J$  and magnetic field are combined and two models for vortex quantum tunneling will be tested against the experimental data. We end in Sec. VII with some conclusions.

## II. JOSEPHSON-JUNCTION ARRAYS

A Josephson array consists of a regular network of superconducting islands weakly coupled by identical tunnel junctions. Compared to films, disorder is weak. With present technology variations in junction parameters are below 20% across the whole 2D array. In addition, different geometries can be fabricated. A square array is obtained by coupling islands to four neighbors and a triangular array by coupling islands to six neighbors. In Fig. 2, we show scanning-electron microscope (SEM) photographs of fabricated square and triangular arrays.

Arrays are made in a planar geometry, in which each island is coupled to a far away ground by its self-capacitance  $C_0$  and to each of the other islands, also through the space outside the 2D plane. Since junctions are made of two overlapping superconducting layers separated by a thin oxide layer, the main contribution to the capacitance comes from the junction capacitance  $C$ . As a result,  $C$  dominates the other elements of the capacitance matrix including  $C_0$ . In Josephson-junction models, the influence of  $C_0$  is taken into account but the other capacitances are usually neglected.

The physics of quantum phase transitions in artificially fabricated Josephson-junction arrays is related to work on thin granular and amorphous (homogeneous) films.<sup>2,3</sup> In

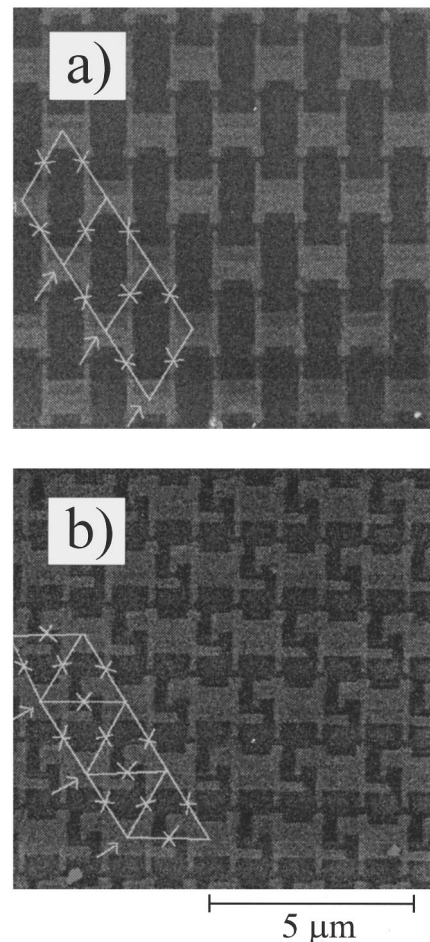


FIG. 2. Scanning-electron microscope photographs of a square (a) and a triangular (b) array. In the photographs, the schematic drawings of the arrays are also shown; crosses represent the junctions and arrows the way current is injected.

granular films, superconducting grains form an irregular pattern, and are coupled by Josephson junctions of different strength. Their self-capacitance to ground is of the same order as the intergrain capacitance. In amorphous films, the normal-state resistance plays the role of the Josephson coupling and the localizing effect on charges of random disorder can be compared to the charging effects in a Josephson-junction array. Near the S–I transition the order parameter itself is suppressed and fluctuations in its amplitude play a role.<sup>2</sup> In contrast, for the fields and temperatures of interest Josephson-junction arrays only exhibit phase fluctuations of the order parameter.

A disadvantage of artificial arrays on the other hand is that finite size effects play a more important role than in films; typical arrays have sizes of 100 by 100 cells. For instance, in classical vortex arrays the Kosterlitz-Thouless-Berezinskii (KTB) phase transition is smeared out. Thermally activated single vortices can cross the array so that a finite resistance is measured below the KTB transition.<sup>21</sup> Another consequence of the small array sizes is that in quantum arrays with  $E_C \approx E_J$  the possibility of vortex tunneling across the whole array width needs to be considered.

When in the classical limit ( $E_C \ll E_J$ ) a magnetic field is applied perpendicular to the islands and junctions, vortices

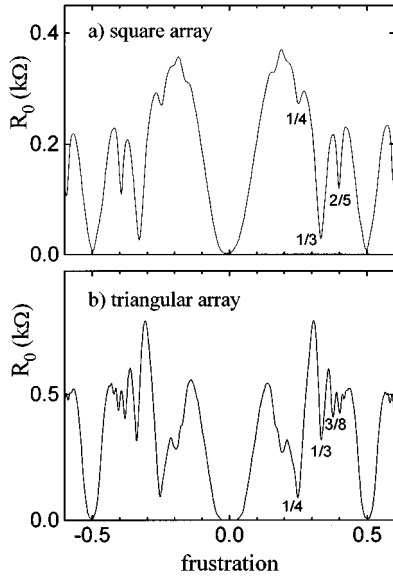


FIG. 3. Zero-bias resistance versus magnetic frustration for a square (a) and triangular array (b). In both graphs the dip at  $f=1/2$  is the most pronounced feature, but in a square array the dip at  $f=1/3$  is more pronounced than the dip at  $f=1/4$  whereas in the triangular array this is the opposite.

enter the array above some small critical field.<sup>21</sup> Just as in films their density increases with increasing magnetic field. In junction arrays the periodic lattice potential prevents vortices to move at low temperatures. However, above the depinning current, there is a flux-flow branch of which the resistance is found to increase approximately linearly with  $f$  up to  $|f|=0.2$ . A phenomenological model<sup>22</sup> analogous to the Bardeen-Stephen model to describe flux-flow in films is in good agreement with experiments providing that enough dissipative damping is present.<sup>23,24</sup>

In larger magnetic fields the behavior of junction arrays is richer than that of films. At fractional values of  $f$  the magnetic vortices form a lattice which is commensurate to the underlying junction network. The stability of the vortex lattice against a bias current leads to a decrease in the small-bias resistance. In order to their relative strength, one expects dips at  $f=1/2, 1/3, 1/4, 2/5, \dots$  in square arrays<sup>25,26</sup> and at  $f=1/2, 1/4, 1/3, 3/8, \dots$  in triangular arrays<sup>27,28</sup> as is illustrated for our arrays in Fig. 3. Near these fractional values of  $f$ , defects from the ordered lattice (excess single vortices or domain walls) are believed to determine the array dynamics in a similar way as the field-induced vortices determine array dynamics near  $f=0$ . Therefore, arrays near commensurate values with high stability such as  $f=1/2$  may qualitatively behave in a similar way as near zero magnetic field. Because all properties are periodic in  $f$  with period  $f=1$  an increase beyond  $f=1/2$  does not lead to new physics.

### III. EXPERIMENTAL DETAILS

Arrays in this study are fabricated of all-aluminum high-quality Josephson-tunnel junctions with a shadow-evaporation technique. The evaporation mask is a three-layer resist system consisting of two electron sensitive resist layers separated by a thin germanium layer. Junctions are formed

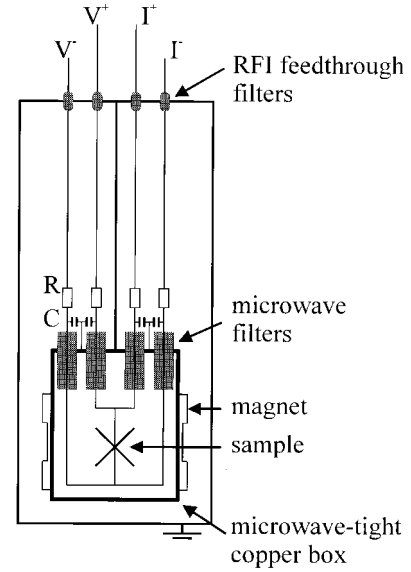


FIG. 4. Schematic drawing of the experimental setup. The RFI-feedthrough filters are at room temperature; the RC and microwave filters are at mixing chamber temperatures.

by evaporating 25 nm aluminum as bottom electrode followed by *in situ* oxidation in oxygen and evaporation of the counter electrode of 50 nm from an opposite angle.<sup>29</sup>

Along their widths, arrays are connected to narrow superconducting strips (busbars). Current is injected through these busbars and they also serve as probes to measure the voltage across the array. To reduce the influence of phase distortions near the busbars, arrays are generally made longer than wide. All our arrays are 190 cells long ( $M=190$ ) and 60 cells wide ( $N=60$ ). A cell of the array has an area ( $S$ ) of  $4 \mu\text{m}^2$  and one island has an area of about  $1 \mu\text{m}^2$ .

We measure the arrays in a dilution refrigerator inside  $\mu$  metal and lead magnetic shields at temperatures down to 10 mK. At the entrance of the cryostat, electrical leads are filtered with radio-frequency interference (RFI) feedthrough filters. Arrays are placed inside a closed, grounded copper box (microwave tight). All leads leaving this box are filtered with RC filters for low-frequency filtering ( $R=1 \text{ k}\Omega$  and  $C=470 \text{ pF}$ ) and with microwave filters. A microwave filter consists of a coiled manganin wire (length  $\sim 5 \text{ m}$ ), put inside an grounded copper tube that is filled with copper powder (grains  $< 30 \mu\text{m}$ ). The resistance of the wire in combination with the capacitance to ground via the copper grains provide an attenuation over 150 dB at frequencies higher than 1 MHz. The copper box with the RC and microwave filters is situated in the inner vacuum chamber and is mounted on the mixing chamber in good thermal contact. The extensive filtering and the copper box are minimum requirements against the influence of high-energy photons from room-temperature electromagnetic noise and radiation.

A small perpendicular magnetic field can be applied by two coils of superconducting wire, placed in a Helmholtz configuration. A frustration of  $f=BS/\Phi_0=1/2$  corresponds to an applied magnetic field of  $B=2.6 \text{ G}$ . The setup is schematically shown in Fig. 4. In Table I, we summarize the characteristics of the arrays that have been measured.

TABLE I. Sample parameters for our square (S) and triangular (T) arrays.

Sample	$R_n$ (k $\Omega$ )	$C$ (fF)	$\beta_c(T=0)$	$E_J/k_B$ (K)	$E_C/E_J$	$\tau_V(f=0)$
S1	36.0	1.1	96	0.21	4.55	
S2	15.3	1.1	17.4	0.50	1.82	
S3	14.5	1.1	15.6	0.53	1.67	(0.28)
S4	11.5	1.1	12.4	0.66	1.25	0.4
S5	10.5	1.1	11.3	0.73	1.11	0.7
S6	5.0	1.1	5.4	1.5	0.56	0.83
S7	8.0	2.0	15.6	0.96	0.48	0.85
S8	6.8	1.7	11.3	1.1	0.45	0.88
S9	2.5	1.1	2.7	3.1	0.27	0.90
S10	3.3	3.5	11.3	2.3	0.14	
S11	1.14	1.1	1.2	6.7	0.13	0.95
T1	25.7	1.2	29	0.30	2.6	1.15
T2	23.8	1.7	39	0.32	1.7	1.6
T3	8.3	1.1	8.7	0.92	0.9	1.51
T4	4.7	1.1	7.2	1.6	0.35	1.85

### A. Junction parameters

The junction capacitance  $C$  determines the charging energy,  $E_C = e^2/2C$ . An independent estimate of  $C$  is obtained from measuring the voltage offset ( $V_{\text{offset}}$ ) at high bias currents at  $T=10$  mK in a magnetic field of 2T. Using the so-called local rule<sup>30</sup> and neglecting possible parasitic contributions (capacitance to ground and capacitances between islands further away)  $C = Me^2/2V_{\text{offset}}$ . We find  $C$  to be 1.1 fF for our smallest junctions of  $0.01 \mu\text{m}^2$ . We have used the local rule instead of the global rule to describe the coupling of tunneling processes to the environment because we measure the voltage offset at high-bias currents in which case the local rule is more applicable. The local rule is commonly used to determine the junction capacitance in small series arrays. From measurements on many small series arrays, variations in the junction area and therefore  $C$  are estimated to be within 20%. Likewise, we estimate the variation in the junction critical current  $I_c$  to be also in the 20% range or less.

The Josephson coupling energy of a junction  $E_J$  [ $=\Phi_0 I_c/(2\pi)$ ] is inversely proportional to the normal-state junction resistance  $R_n$ .  $R_n$  follows from the normal-state array resistance  $r_n$  measured at 4.2 K,  $R_n = (N+1)r_n/M$ . The maximum junction critical current in the absence of charging effects and thermal fluctuations ( $I_c$ ) is assumed to be given by the Ambegaokar-Baratoff value<sup>31</sup> with a measured critical temperature  $T_c$  of 1.35 K. At low temperatures,  $I_c R_n = 322 \mu\text{V}$ . The degree of damping in junctions is commonly defined through the McCumber parameter  $\beta_c(T) = 2\pi I_c(T) C R_e^2 / \Phi_0$ , where  $R_e$  is the effective damping resistance for each junction. In Table I, we have listed the value of  $\beta_c(0)$  calculated with  $R_e = R_n$ .

One should realize that there is a lower limit to the junction normal-state resistance. For small junctions with low  $R_n$ , the oxide barrier is of the order of one atomic layer. Such thin layers may produce leaky junctions. We find that for our 1 fF junctions, this lower limit is about 1 k $\Omega$ . Thus, our aluminum tunnel junctions may become leaky when

$R_n C < 10^{-12}$  s. For very small junctions with  $C < 0.1$  fF, this criterion indicates that  $R_n > R_q$  ( $=h/4e^2 = 6.45$  k $\Omega$ ).

### B. Array properties

Many array properties depend on the ratio between the Josephson and the charging energy. In comparing properties of square and triangular arrays some care is necessary. The actual energy required to store an additional electron on an island is  $e^2/2C_\Sigma$ , where  $C_\Sigma$  is the sum of the capacitances to other islands and to ground. As in triangular arrays all islands are coupled with  $z=6$  instead of  $z=4$  junctions, the energy required is 2/3 times smaller than that of an island in a square lattice. Similarly, the freedom of the phase on a particular island is determined by the Josephson coupling energy of all junctions connected to the island and therefore it seems reasonable to assume that in a triangular array the effective Josephson coupling energy is 3/2 times that of a square array. To take these effects into account we define an effective ratio  $x = (E_C/E_J)_{\text{eff}}$ . In a square array  $x = E_C/E_J$  but the corresponding value in a triangular array is defined as  $x = 4E_C/9E_J$ . Different  $x$  ratios are obtained by varying  $R_n$  while keeping  $C$  in the order of 1–3.5 fF. In this paper, we present data on arrays with  $R_n$  values ranging from 1 to 36 k $\Omega$  and  $x$  ranging from 0.1 to 4.6. Apart from systematic errors that are the same for all samples (such as the use of the local rule to determine  $E_C$ ), we estimate our error in determining  $E_C/E_J$  to be 10%.

The self-capacitance  $C_0$  of individual islands is estimated from separate measurements on small series arrays with high  $E_C/E_J$  ratio. A magnetic field of 2 T is applied so that the series arrays are in the normal state.  $C_0$  is measured by varying the potential of the circuit with respect to the ground potential. Recording the current through the circuit yields a periodic signal with period  $e/C_0$ . For islands of  $1 \mu\text{m} \times 1 \mu\text{m}$ ,  $C_0 \approx 12 \times 10^{-18}$  F. We take this value of 12 aF as an estimate for  $C_0$  in our 2D arrays.

In small series arrays it is known that all islands carry random offset charges that are presumably caused by defects

in the junctions or substrate. Electron or quasiparticle tunneling will partly compensate these offset charges so that their value lies between  $-e/2$  and  $+e/2$ . These charges can be nulled out by the use of a gate for each island. In a 2D array similar offset charges are expected. Here in practice they cannot be compensated because too many gate electrodes would be necessary, requiring complicated fabrication procedures. Therefore, some degree of disorder is intrinsically present in our arrays but only near the S–I transition and on the insulating side will this charge disorder affect physical properties. The presence of the frozen-in offset charges also means that a uniform charge frustration is difficult to realize experimentally.

In the description of phase transitions in 2D superconducting systems, the influence of dissipation needs to be taken into account. In a single small junction, the high-frequency coupling to the environment determines the effective damping, yielding an effective impedance of the order of  $100 \Omega$ . This impedance can be increased, i.e., a single junction can be decoupled from its environment by placing high-ohmic resistors or arrays of small junctions in the leads close to the junction. From the latter we expect that junctions inside a 2D array are decoupled from the leads.

At low temperatures one would not expect quasiparticle tunneling to play a role in our samples since  $E_c$  is smaller than the superconducting gap  $\Delta$ . Experiments on small arrays, however, indicate that even at milliKelvin temperatures a small but finite amount of quasiparticles is always present. This is apparent, for example, in the vortex interference experiment<sup>4</sup> where vortices move around a charge with the periodicity  $e$  instead of  $2e$ . The quasiparticles may be generated by the environment (e.g., by photons).

Quasiparticles may also be generated by the moving vortices themselves. When vortices cross junctions, the junction-phase difference changes abruptly by  $\pi$  in square arrays and  $4\pi/3$  in triangular arrays. According to the Josephson relation, these phase changes lead to voltage spikes of which the amplitude depends on the time the vortex spends crossing the junctions. Precise values of this time are not known. Nevertheless, due to the highly nonlinear character of the junction dynamics, coupling to voltages larger than  $\Delta/e$  can be expected and hence the creation of quasiparticles. This mechanism of quasiparticle generation is a result of the discrete nature of Josephson arrays. It would therefore be difficult to eliminate quasiparticles completely.

Tunneling of quasiparticles leads to dissipation characterized by the dimensionless parameter  $\alpha_e = R_q/R_e$ . This  $R_e$  cannot be smaller than  $R_n$  nor larger than the subgap resistance. In tunnel junctions at low temperatures, the subgap resistance is orders of magnitude larger than  $R_n$ . It is important to realize that the parameter  $\alpha_n = R_q/R_n$  is not independent of the  $E_c/E_J$  ratio because  $E_c/E_J = (2E_c/\Delta)\alpha_n^{-1}$ .

At low temperatures, the 2D flux penetration depth  $\lambda_{\perp}(T) = \Phi_0/2\pi\mu_0 I_c(T)$  is much larger than the array sizes so that the magnetic field is essentially uniform over the whole array. Thus, self-induced magnetic fields can be neglected in our arrays. A similar conclusion can be drawn by considering the ratio of the cell inductance (we estimate the geometrical inductance to be of the order of 1 pH) to the Josephson inductance ( $>1$  nH).

#### IV. S–I TRANSITIONS AS A FUNCTION OF $E_c/E_J$

In zero magnetic field, classical arrays undergo a Kosterlitz-Thouless-Berezinskii (KTB) phase transition<sup>32</sup> to the superconducting state. Below the KTB transition temperature  $T_V \sim E_J/k_B$ , arrays are superconducting because there are no free vortices. Only pairs of vortices and antivortices may be present. A necessary condition for a clear observation of a KTB phase transition is that vortices interact logarithmically over large distances. In arrays, vortices interact logarithmically over distances  $\lambda_{\perp}$ .

When  $E_c \gg E_J$ , a dual KTB transition for  $2e$  charges is expected at a transition temperature  $T_C \sim E_c/4k_B$ .<sup>14,33,34</sup> When only  $C_0$  is considered  $2e$ -charge pairs interact logarithmically over a normalized screening length of  $\sqrt{C/C_0}$ . In our arrays,  $\sqrt{C/C_0} \approx 10$  so that the KTB transition will be smeared out. However, when the full capacitance matrix is considered logarithmic interactions persist over lengths of order  $C/C_0$ ,<sup>1,35</sup> i.e., of the order of the array size. Therefore, one expects to observe the distinct features of a KTB transition for charges in our arrays.

At  $T=0$  in zero field, theoretical studies indicate a S–I transition as a function of the  $E_c/E_J$  ratio. Quantitative studies have mostly been concentrated on infinite, square arrays in the absence of disorder. From duality arguments, Fazio and Schön<sup>14</sup> have estimated the critical value  $x_{cr}$  separating superconducting and insulating behavior at  $T=0$ . In the absence of damping, their analysis gives  $x_{cr} = \pi^2/2a$ . The factor  $a$  arises from a symmetry breaking term, i.e., from the spin-wave contribution to the charge correlation function ( $a \geq 1$ ). In the presence of quasiparticles arrays with strong dissipation ( $\alpha_e > 0.45$ ) are expected to be in the superconducting state at  $T=0$ .<sup>1</sup> Other authors have used other methods to calculate  $x_{cr}$ . Analytical calculations<sup>36</sup> yield  $x_{cr} \approx 10$ , a variational approach<sup>37</sup>  $x_{cr} \approx 2$ , and two studies based on Monte Carlo simulations indicate that  $x_{cr} \approx 1.7$ ,<sup>38</sup> and  $x_{cr} \approx 3$ .<sup>39</sup>

In superconducting films as well as in arrays, it has also been argued that the zero-temperature resistance  $R_0^*$  at the critical point is finite so that the array acts like a metal right at the S–I transition.<sup>13</sup> From the vortex-charge duality one expects the resistance per junction to be the quantum resistance of pairs,  $R_q$ . This value of the resistance can be thought of as due to the simultaneous passing of one Cooper pair and one vortex through the system. More detailed calculations on short-range interacting bosons on a 2D lattice (Bose-Hubbard model) have shown that in the absence of disorder and dissipation  $R_0^*$  has a universal value of  $8R_q/\pi$  per square.<sup>40</sup> When resistive shunting of the junctions is included,  $R_0^*$  is expected to be higher and equal to  $R_q/0.12$  per square.<sup>20</sup>

In a magnetic field of  $f=1/2$  in the absence of resistive shunts, the zero-temperature critical behavior of the square XY model has been analyzed by Granato and Kosterlitz.<sup>41</sup> They find that here  $R_0^*$  has a universal value of  $4R_q/\pi$ , half the value of the zero-field critical resistance. Recent calculations<sup>42</sup> on the Bose-Hubbard model in a magnetic field show that  $R_0^* = 1.9R_q$  at  $f=1/2$  and  $R_0^* = 1.2R_q$  at  $f=1/3$ .

##### A. Experiments at $f=0$

Figure 5 shows the resistive transitions of six different square arrays in zero magnetic field. The zero-bias resistance

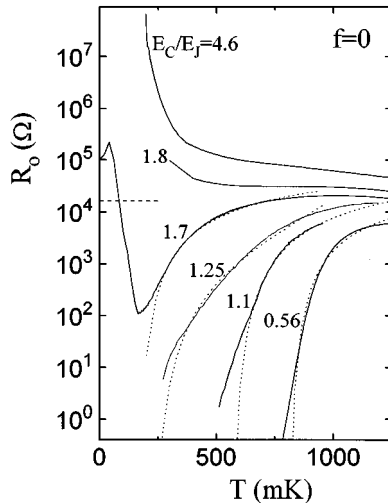


FIG. 5. The zero-field linear resistance per junction measured as a function of temperature for six different arrays. Dotted lines are fits to the vortex-KTB square-root cusp formula. The dashed horizontal line shows the zero-temperature universal resistance ( $8R_q/\pi=16.4$  k $\Omega$ ) of the S–I transition at  $f=0$ .

per junction ( $R_0$ ) is measured with a very small transport current ( $<10^{-3}I_c$  per junction) in the linear part of the current-voltage characteristic. Three arrays become superconducting, two arrays insulating and one array that lies very close to the S–I transition shows a double reentrant dependence. The horizontal dashed line in Fig. 5 is the critical resistance value of  $8R_q/\pi$ .

For the three arrays that become superconducting, we have fitted our data to the predicted square-root cusp dependence on temperature,  $R_0/R_n=c \exp[-b/(\tau-\tau_V)^{1/2}]$  with  $b$  and  $c$  constants of order one. To compensate for the temperature dependence of  $E_J$ , a normalized temperature is defined as  $\tau=k_B T/E_J$ . From these fits we have determined the normalized KTB transition temperature  $\tau_V$  for our arrays. Results are listed in Table I. We find that near the S–I transition  $\tau_V$  is substantially smaller than the classical value of 0.90. Note that at low resistance levels ( $R_0 < 10^{-3}R_n$ ), deviations from the square-root cusp dependence are found and that the resistance decreases exponentially. As mentioned in Sec. II, this is indicative of thermal activation of single vortices across the whole array width.

Two arrays become insulating, showing a continuous increase of  $R_0$  as  $T$  is lowered. From the vortex-charge duality, one now expects the conductance to follow a square-root cusp dependence on temperature. We do not observe this square-root cusp dependence characteristic for the KTB transition. Instead we observe an exponential decrease of the conductance. The activation barrier is equal to  $0.25E_C+\Delta$ . The same exponential behavior with exactly the same barrier has been reported by the Harvard and Chalmers groups.<sup>17,18</sup>

This exponential decay can be explained as thermal activation against the sum of two barriers: the superconducting energy gap ( $\Delta$ ) to break a Cooper pair and  $E_C/4$  to separate this pair to create a charge anticharge pair on two adjacent islands. Like with vortices in arrays at the superconducting side of the S–I transition, one expects that separating this pair further apart would lead to an additional term to the

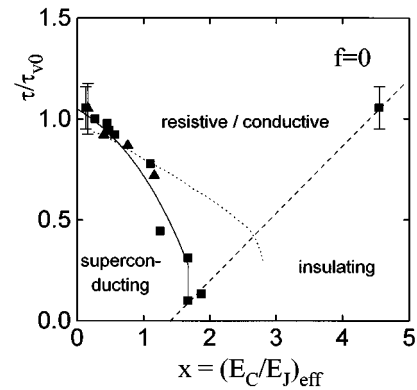


FIG. 6. Measured phase diagram of our square arrays (solid squares) and triangular (solid triangles) in zero magnetic field, showing the superconductor-to-insulator transition at  $(E_C/E_J)_{\text{eff}} \approx 1.7$ . The solid line is a guide to the eye connecting the data points and the dotted line at the superconducting side is the result of a recent calculation (Ref. 39).

energy barrier proportional to the logarithm of their separation. The absence of this logarithmic term indicates that the interaction is screened at lattice spacing distances. This enhanced screening is not understood yet.

The resistance of sample *S3* has a very remarkable dependence on temperature. Starting at high temperatures,  $R_0$  first decreases when the temperature is lowered. Over two orders of magnitude it follows the square-root cusp expression. Below  $T=150$  mK, however,  $R_0$  increases by more than three orders of magnitude and at the same time a charging gap develops in the  $I$ - $V$  curve. Finally at 40 mK,  $R_0$  starts to decrease again. The second reentrant transition at 40 mK seems to be a more general feature of arrays near the S–I transition which is also present in a magnetic field. Different explanations for reentrant transitions from S-like to I-like behavior have been proposed in the literature.<sup>20,43–46</sup> In the absence of quantitative predictions, we cannot discriminate between the different theories.

Summarizing the zero-field results we have plotted our data in a phase diagram and compared this with theoretical predictions. In Fig. 6 the superconducting–normal phase boundary is the vortex-KTB phase transition. Temperature on the vertical axis in this figure is given in units of  $\tau=k_B T/E_J$  and scaled to  $\tau_{V0}$ , the KTB transition temperature in the classical limit  $x=0$ . We find  $\tau_{V0}=0.95$  for our square arrays which is close to the value of 0.90 determined from Monte Carlo simulations.<sup>25</sup> For our triangular arrays,  $\tau_{V0}=1.7$  which should be compared to the Monte Carlo value of 1.45.<sup>27</sup> As a function of  $x$  a clear, systematic decrease of the KTB transition temperatures is observed. In the insulating side of the figure no phase transition was observed. The dashed line therefore is somewhat arbitrary. It represents the crossover to the low-temperature region with  $R_0 > 10^3 R_n$ .

Our measurements indicate that  $x_{\text{cr}} \approx 1.7$ . This value is in agreement with the Monte Carlo simulations and the calculations based on the variational approach. The calculation based on duality arguments agrees with our experiments if  $a \approx 3$ .

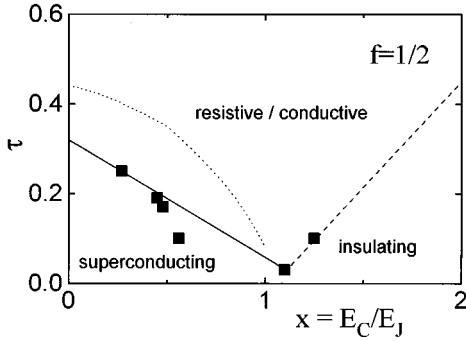


FIG. 7. Measured phase diagram of our square arrays at  $f=1/2$ , showing the superconductor-to-insulator transition at  $E_C/E_J \approx 1.2$ . The solid line is a guide to the eye and the dotted line at the superconducting side is the result of a recent calculation (Ref. 39).

In the quantum Monte Carlo study of Ref. 39, the reduction of  $\tau_V$  has been calculated as a function of  $x$ . The dotted line in Fig. 6 is the result of this study. The calculations show a larger value of  $x_{cr}$  but there is a good agreement between the calculations and the experiment for small  $x$ . Here, the reduction of the KTB transition temperature follows the expression  $\tau/\tau_{V0} \sim 1 - 2.9x/z^2$  where  $z$  is the number of neighboring islands. This expression indicates that  $\tau/\tau_{V0}$  of triangular arrays and square arrays are expected to coincide if the  $x$  values for the triangular arrays are scaled with  $16/36$ . This is in fact the scaling we used for our experimental points in Fig. 6.

For our 1 fF junctions, the S–I transition of Fig. 6 could have been induced by dissipation. Suppose  $R_e = \gamma R_n$  with  $\gamma \geq 1$ . Then, the criterion  $\alpha_e > 0.45$  translates into  $E_C/E_J < 2\gamma$ , i.e.,  $x_{cr} = 2\gamma$ . To match our experimental data,  $\gamma$  has to be 1. Thus, our data do not exclude the possibility that the S–I transition is influenced by the normal-state resistance. Any other resistance value for the damping can be ruled out. A systematic study on samples with larger capacitances could be used to test this influence; arrays with 5 fF junctions should have a critical  $E_C/E_J$  ratio of 0.4 if the transition is driven by dissipation with  $R_n$  as damping resistance.

### B. Experiments at commensurate $f$ values ( $f=1/2, 1/3$ )

We have measured the S–I transition of square arrays at  $f=1/2$  in detail and in Fig. 7 its experimental phase diagram is shown. At  $f=1/2$  the interaction between domain-wall excitations with  $1/4$  fractionally charged vortices at the corners and excess single integer vortices is believed to trigger a combined KTB-Ising transition. The classical Monte Carlo simulations indicate a transition temperature of  $\tau=0.44$  for  $x=0$ .<sup>25</sup>

As in  $f=0$ , our measurements indicate a superconductor-to-insulator transition at  $T=0$ . From  $R_0(T)$  curves we find a S–I transition for  $f=1/2$  which occurs around 11 k $\Omega$  (at low temperatures, sample *S5* becomes superconducting, whereas sample *S4* becomes insulating). The critical  $E_C/E_J$  ratio is about 1.2, a factor 0.7 lower than the zero-field value. This decrease of  $x_{cr}$  is consistent with the simple model that at  $f=1/2$  the effective Josephson coupling energy is modified: the interaction energy of a vortex pair is a factor  $\sqrt{2}$  smaller than in zero field. With this lower effective coupling the  $x$

value of the S–I transition is shifted by  $2^{-1/2}$ , which is close to the observed reduction of 0.7.

Like in the  $f=0$  case, the dashed line in Fig. 7 is the result of quantum Monte Carlo calculations.<sup>39</sup> For  $x \rightarrow 0$ , the calculated values extrapolate to the expected value of 0.44. The experimental points of the transition temperatures are lower than the calculated ones. At present, we have no explanation for this discrepancy. It would require a more detailed study and better understanding of the phase transition at  $f=1/2$ . The calculations do indicate, on the other hand,  $x_{cr} \approx 1$ , in agreement with the experiment.

There are no detailed calculations yet for the phase transition at other commensurate fields. At  $f=1/3$  in array *S5* we find a double reentrant dependence of the resistance similar to the curve of sample *S3* in Fig. 5. The minimum and maximum resistances occur at the same temperatures but the resistance only varies between 3.8 and 5.5 k $\Omega$ . This array lies very close to the S–I transition for this value of  $f$ , so that  $x_{cr} \approx 1.1$  and  $R_0^* \approx 4.5$  k $\Omega$  at  $f=1/3$ . Note, that at  $f=1/2$  array *S5* becomes superconducting when lowering the temperature.

## V. FIELD-TUNED TRANSITIONS

In arrays which are in the superconducting state at  $f=0$  but have an  $(E_C/E_J)_{eff}$  ratio close to the critical value, a magnetic field can be used to drive the array into the insulating state. This field-tuned transition has been considered theoretically by Fisher<sup>12</sup> in disordered systems and has been observed<sup>47</sup> in  $\text{InO}_x$  films. At low magnetic fields vortices at  $T=0$  are pinned but for higher fields, the vortex density increases and at some critical density, vortices Bose condense. The vortex superfluid leads to an infinite resistance. The charge-vortex duality near the S–I transition indicates that this transition can also be thought of as Bose condensation of charges that occurs with decreasing magnetic field. In Josephson-junction arrays with  $E_C \approx E_J$  disorder is introduced by the random offset charges and therefore we believe that the predictions of the critical behavior are also adequate for our Josephson system.

The general characteristic of this S–I transition is that when  $f$  is increased from zero, the temperature derivative of the resistance changes sign at critical values  $\pm f_c$ . This is visible in the  $R_0(T)$  plots of Fig. 8. Below a critical value  $f_c$ , the resistance decreases upon cooling down ( $dR_0/dT > 0$ ). Above  $f_c$  the resistance increases ( $dR_0/dT < 0$ ) and for low temperatures reaches a value that might be orders of magnitudes higher than the normal-state resistance. This sign change in the temperature dependence corresponds to a change in the  $I$ - $V$  characteristics shown in Fig. 1(b).

### A. Scaling behavior

A detailed way of observing this field-tuned S–I transition is by measuring the resistance versus magnetic field for different temperatures. For sample *T2* the result is shown in Fig. 9. In the range  $0 < f < 1/3$ , the  $R(f)$  curves are very similar to the ones measured in thin films. Below the critical field  $f_c=0.14$  the resistance becomes smaller when the temperature is lowered and above  $f_c$  the resistance increases. In

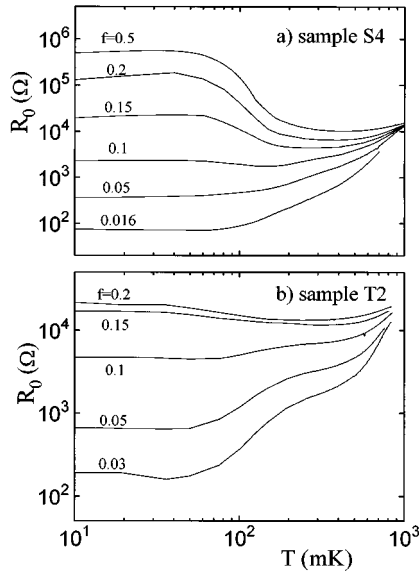


FIG. 8. The linear resistance per junction of array S4 (a), and array T2 (b) measured as a function of temperature for various values of the magnetic field. The field-tuned S–I transition occurs at that frustration where the temperature dependence of  $R_0$  changes sign. For both arrays this sign change occurs between  $f=0.10$  and  $f=0.15$ .

Table II we give the values of  $f_c$  and  $R_0$  for the two square and the two triangular samples that showed field-tuned transitions.

According to Fisher,<sup>12</sup> the slopes of the  $R(f)$  curves at  $f_c$  should follow a power-law dependence on  $T$  with power  $-1/(z_B \nu_B)$ . The exponents  $z_B$  and  $\nu_B$  characterize the scaling behavior of the field-tuned S–I transition. When on a double logarithmic plot the slopes of the  $R(f)$  curves at  $f_c$  are plotted versus  $1/T$ , we find a straight line in the temperature range  $50 < T < 500$  mK, as shown in Fig. 10 for sample T2 and S5. From the reciprocal of this straight line the product  $z_B \nu_B$  can be determined. In different samples, we find values between 1.2 and 2 as listed in Table II. These values are consistent with measurements by others on Josephson-

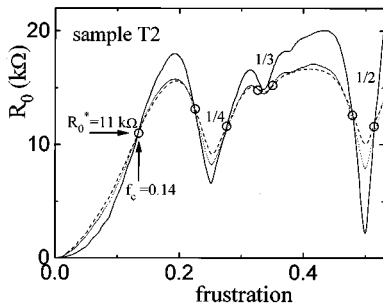


FIG. 9. The linear resistance per square of array T2 measured as a function of the magnetic field for three different temperatures,  $T=50$  mK (solid line), 120 (dotted), and 160 (dashed) line). Below the critical field  $f_c$ , the resistance decreases when  $T$  is lowered; above  $f_c$  in the range  $f_c < f < 0.25$  the resistance increases. Near fractional values of  $f$  additional field tuned transition can be observed.

TABLE II. Critical exponents and resistances of the field-tuned transitions.

Sample	$f_{\text{comm}}$	$f_c$	$R_c$ (k $\Omega$ )	$z_B \nu_B$
S4	0	0.1	2.5	1.2
S5	0	0.22	2.5	1.5
	1/3	0.015	4.6	0.6
	1/2	0.05	3.4	1.2
T1	0	0.02	4.5	(4.4)
T2	0	0.14	11	2.1
	1/4	0.025	12–13	0.8
	1/3	0.01	15	
	1/2	0.02	12	0.7

junction arrays,<sup>11</sup> with the values found in InO<sub>x</sub> films<sup>47</sup> and high- $T_c$  films<sup>48</sup> as well as with the theoretical expectations ( $z_B=1$  and  $\nu_B \geq 1$ ).

The exponent  $z_B$  can also be obtained from the measurements by plotting  $f_c$  as a function of the zero-field KTB transition temperature,  $f_c \propto T_V^{2/z_B}$ . Our two data points on the triangular arrays yield a rough estimate of  $z_B \approx 0.34$  and the two data points on the square arrays of  $z_B \approx 1.4$ .<sup>49</sup>

In the original paper by Fisher<sup>12</sup> the resistance per square at the transition is predicted to be universal and of the order of  $R_q$ . Measurements on different thin films show that the resistance right at the transition is of the order of  $R_q$  but measurements are not conclusive regarding the universality. In our arrays, this resistance is again of order  $R_q$ , yet it varies between 2.5 and 12.5 k $\Omega$  (see Table II). For triangular arrays, one should probably take the resistance per square which is 0.5 times the junction resistance. In that case, the critical resistance at the transition varies between 2.5 and 6 k $\Omega$ .

A new feature introduced by Josephson-junction arrays is the existence of field-tuned transitions near commensurate values of the applied field, i.e., at  $f_{\text{comm}} \pm f_c$ .<sup>10,11</sup> Studying the  $R(f)$  curves of sample T2 in more detail, we see critical behavior not only around  $f=0$ , but also around  $f=\pm 1/4$ ,  $\pm 1/3$ ,  $\pm 1/2$ ,  $\pm 2/3$ , and  $\pm 3/4$ . Thus, in this sample in total 12 critical points can be observed when going from  $f=0$  to  $\pm 1$ . For sample S5, similar transitions occur near  $f=\pm 1/3$ ,  $\pm 1/2$ , and  $\pm 2/3$ . For each commensurate  $f$  value  $z_B \nu_B$  can be de-

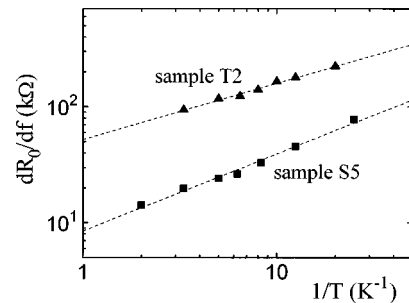


FIG. 10. The slopes of the  $R(f)$  curves at  $f_c$  plotted as a function of the inverse temperature for a square and triangular sample. The slope of the dashed lines determines the product of the critical exponents  $z_B \nu_B$ .

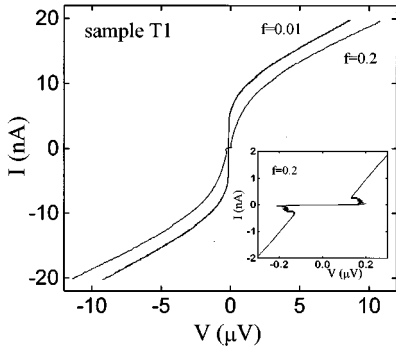


FIG. 11. Two current-voltage characteristics of sample *T1* measured in a field below  $f_c$  ( $f=0.01$ ) and above  $f_c$  ( $f=0.2$ ). Inset: the current-voltage characteristic measured at  $f=0.2$  on an expanded scale showing the “Bloch nose” at the edge of charging gap.

terminated as described above. In Table II we list the results for sample *T2* and *S5*. For *T2*, we find values of  $z_B \nu_B$  around 1 and critical-resistance values of 11 k $\Omega$ . For the square array *S5*, the values of  $z_B \nu_B$  are about the same, but the critical resistance is a factor of 3 smaller. Calculations on the boson Hubbard model in a magnetic field<sup>42</sup> show that the product  $z_B \nu_B$  at  $f=1/2$  is close to 1 in agreement with our measurement.

### B. $I$ - $V$ characteristics

The changing nature of the  $I$ - $V$  characteristic at the S–I transition is shown in Fig. 11 in more detail and once more illustrates the competing dynamics of vortices and charges. Below  $f_c$  the  $I$ - $V$  shows a supercurrent branch with a finite slope. When on the other hand the field is increased above  $f_c$ , a small charging gap opens up in the supercurrent branch. The zero-bias conductance is measured within this gap and is temperature independent for  $T < 50$  mK. We attribute this metallic behavior on both sides of the S–I transition to quantum tunneling of vortices and charges, respectively. We do not expect the metallic behavior to be due to an effective noise temperature of 50–100 mK in our heavily filtered setup, because several samples do show a changing resistance below these temperatures.

The metallic behavior is not in contradiction with the picture of Bose condensation as discussed in the beginning of this section. Consider for instance, the tunneling of vortices at the superconducting side of the S–I transition. With a small current applied and in the absence of damping, a tunneled vortex would accelerate up to high velocities. When its kinetic energy equals the gap energy, many quasiparticles will be generated and damping will suddenly become important. This process would lead to a highly nonlinear  $I$ - $V$  characteristic in contrast to our experimental findings of a linear  $I$ - $V$  around  $V=0$ . The experiments therefore show that moving vortices always experience some damping independent of their velocity. As discussed before in Sec. III B, this damping is caused by the presence of quasiparticles. The finite slope in the charging gap can be understood likewise.

On a large scale, the two  $I$ - $V$ 's of Fig. 11 look similar. Above  $f_c$ , a small charging gap appears in the  $I$ - $V$  characteristic but at high currents and/or voltages the curve still

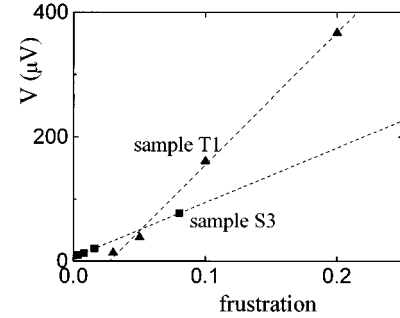


FIG. 12. The width of the gap of a square and triangular array measured as a function of the frustration  $f$ .

looks like an  $I$ - $V$  measured at the superconducting side of the transition. With a small measuring current the resistance is much larger than in the normal state, but with a large measuring current the resistance is smaller. Studies on granular Al films have shown a similar electric-field tuned S–I transition; a dc bias current and/or voltage was used to overcome the Coulomb barrier and at least partly recover Josephson tunneling.<sup>50</sup>

Just above the threshold field, the voltage across the array decreases with increasing current as illustrated in the inset of Fig. 11. In a single junction such a negative resistance is known as the “Bloch nose”.<sup>6,51</sup> It is caused by a macroscopic quantum effect due to the energy band structure for the junction charge states; for low currents, the  $I$ - $V$  follows a high resistance branch (quasiparticle tunneling), but at higher currents coherent Cooper pair tunneling processes (Bloch oscillations) become important and decrease the averaged voltage across the junction. Then for larger currents, Zener tunneling causes the voltage to increase again.

For larger fields the gap becomes more pronounced and we find that the gap width increases linearly with  $f$  as shown in Fig. 12. The gap width is periodic in  $f$ . Theoretical studies on the Bose-Hubbard model have considered the width of this charging gap.<sup>20</sup> The gap at  $T=0$  is proportional to  $\sqrt{f}$ . At nonzero temperatures or in the presence of offset charges, the gap is expected to be linear in  $f$  as observed in our experiment. The absolute value of the gap is much smaller than calculated without the presence of offset charges.

## VI. DISCUSSION

Our results indicate that quantum S–I transitions occur as a function of the  $E_c/E_J$  ratio and applied magnetic field. The critical resistance and critical  $E_c/E_J$  ratio of these S–I transitions depend on the magnetic field, i.e.,  $R_0^* = R_0^*(f)$  and  $x_{cr} = x_{cr}(f)$ . In subsection A we combine our results of these two S–I transitions and try to draw some general conclusions.

For noncommensurate values of  $f$ , our data indicate a superconductor–normal–insulator transition at  $T=0$ . For  $T < 100$  mK, the array resistance of arrays “around” the S–I transition is independent of temperature due to quantum tunneling of vortices/charges. In subsection B, we have collected data of samples at the superconducting side of the S–I transition and compared them to two quantum tunneling models.

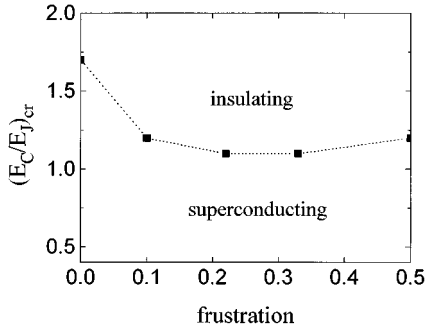


FIG. 13. Measured phase diagram for square arrays in a magnetic field. A sample with a certain  $E_C/E_J$  ratio corresponds to a horizontal line in this figure. Below the dotted line, samples become superconducting at low temperatures; above this line samples become insulating. At noncommensurate magnetic fields, the S–I transition is not sharp because the superconducting region is separated from the insulating region by a metallic region (this additional normal phase is not shown in the figure).

#### A. Critical properties of the S–I transitions

In Fig. 13, we have plotted the critical  $E_C/E_J$  ratio as a function of applied magnetic field for our square arrays. We have combined the three points at  $f=0$ ,  $1/2$ , and  $1/3$  with the two data points of the field-tuned S–I transition. After a rapid decrease the critical ratio is almost constant for  $f>0.1$ . The critical  $E_C/E_J$  ratio at  $f=1/2$  is larger than at other nearby values of  $f$ , indicating once again the stability of the phase configuration at  $f=1/2$ . Figure 13 also shows that arrays in the range  $1.2 < E_C/E_J < 1.7$  do not show special behavior at commensurate  $f$  values (e.g., dips in the magnetoresistance); arrays are superconducting in zero field but insulating at  $f=1/2, 1/3, 1/4, \dots$ .

One expects the magnetic field to effectively lower  $E_J$  so that the S–I transition is shifted to lower  $E_C/E_J$  ratios. A magnetic field also has a stronger influence in triangular arrays because the total phase difference around a cell induced by the flux is divided over three junctions instead of four. In particular, this would mean that in a magnetic field the phase boundary of Fig. 12 is different for triangular arrays; most likely it will lie below the line of Fig. 12. Our measurements are in agreement with this picture.

For the S–I transition at zero field, at commensurate  $f$  values as well as for the field-tuned transitions it has been argued that the zero-temperature resistance right at the transition should be universal. Of course zero temperature cannot be reached in an experiment nor is the sample of infinite size, but extrapolation of our data can still be used as an estimate for the zero-temperature behavior. For the transition in zero field, we find for an array that lies almost on the S–I transition, double reentrant behavior around the predicted resistance value of  $8R_q/\pi=16.4$  k $\Omega$ . For the field-tuned transitions, the critical resistance per square is again of the order of  $R_q$  but varies from 2.5 to 6 k $\Omega$ . In Fig. 14, we have plotted the critical resistance per square for all our S–I transitions together with four points taken from field-tuned transitions measured in Chalmers.<sup>11</sup> As can be seen, the critical resistance varies with  $f$ . Interestingly, the data seem to indicate a dependence of the critical resistance per square that goes as the number of vortices per cell ( $=f$ ) times the critical resis-

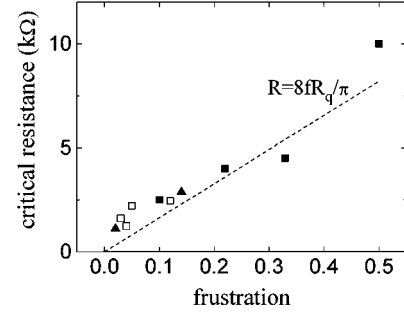


FIG. 14. The critical resistance per junction versus applied magnetic field for our arrays (solid symbols) as well as for four square arrays (open squares) from a study at Chalmers (Ref. 11).

tance ( $=8R_q/\pi$ ). The dashed line indicates a resistance per square and per vortex that is “universal” and equal to  $8R_q/\pi$ . The data are not conclusive since error margins are large.

#### B. Metallic behavior at noncommensurate $f$ values

In a noncommensurate magnetic field ( $0 < f < 0.2$ ), all our “superconducting” arrays show a region with exponential decay of the resistance. We have fitted our data in this regime to a standard Arrhenius form with a frustration-dependent energy barrier

$$R_0(\tau) = c_1 R_n e^{(-\gamma(f)/\tau)}. \quad (1)$$

An example of such a fit is shown in Fig. 15. In Table III, we summarize the results of our samples giving the values of  $\gamma(f)$  and  $c_1$  for  $f=0.1$  of all samples that showed a flattening off of the resistance and for some  $f$  values of one square and triangular array in particular.

Below a certain critical temperature of about 100 mK ( $1/\tau \approx 10$  in Fig. 15) the resistance becomes temperature independent and remains finite down to the base temperature of 10 mK of our dilution refrigerator. In Table III we have also listed the values of the finite resistance per junction ( $R_{00}$ ). We checked that varying the measuring current made no difference in  $R_{00}$  so that self-heating effects can be excluded.

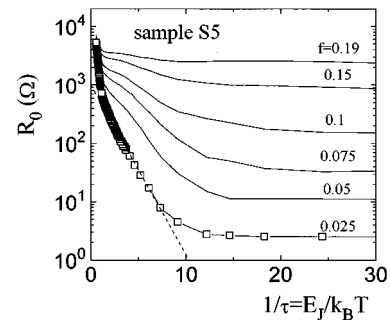


FIG. 15. The linear resistance per junction of sample S5 versus inverse normalized temperature measured for various values of the applied magnetic field. At high temperatures, the resistance decreases exponentially; at low temperature the resistance is temperature independent indicative for quantum tunneling of vortices.

TABLE III. Summary of the resistive behavior of “superconducting” arrays close to the S–I transition.  $\gamma(f)$  and  $c_1$  describe the exponential behavior at high temperature, where  $\gamma(f)$  is the energy barrier in units of  $E_J$ .  $R_{00}$  is the value of the temperature-independent resistance at low temperatures. The listed value is the resistance per junction. The exponents of the tunnel rates which follow from the measurements, are given by  $s_{\text{meas}}$ .  $s_{\text{sv}}$  is the calculated value in the single vortex model as discussed in the text [Eq. (3)].

Sample	$f$	$\gamma(f)$ ( $E_J$ )	$c_1$	$R_{00}$ ( $\Omega$ )	$s_{\text{meas}}$	$s_{\text{sv}}$	$s_{\text{meas}}/s_{\text{sv}}$
S4	0.1			2200			
S5	0.025	0.7	0.1	2.6	10.2	2.6	3.9
	0.05	0.5	0.3	11	9.4	2.3	4.0
	0.075	0.4	0.5	35	8.6	2.2	4.0
	0.1	0.3	0.4	150	7.4	2.0	3.8
	0.15	0.1	0.4	850	6.0	1.4	4.3
	0.19	0.05	0.3	2300	5.1	1.2	4.4
S6	0.1	0.5	0.7	22	9.4	3.7	2.6
S7	0.1	1.8	0.1	0.02	16.7	5.7	2.9
T2	0.1	0.1	0.4	5067	3.5	0.7	5.1
T3	0.03	1.0	0.2	6.8	9.4	2.7	3.5
	0.05	0.5	0.2	74.6	7.4	2.1	3.6
	0.075	0.3	0.3	392	6.0	1.7	3.5
	0.1	0.2	0.4	746	5.7	1.5	3.8
	0.125	0.2	0.5	1057	5.5	1.5	3.6

While at higher temperatures vortices are expected to be mobile due to thermal fluctuations, classically one would expect them to be pinned in the lattice at 10 mK. The fact that we find a finite resistance at those temperatures signifies that there exists a quantum transport mechanism for vortices analogous to quantum tunneling of the phase in single junctions. The exponential behavior at higher temperatures and the flattening off of the resistance at low temperatures fits well with the description of a single quantum-mechanical particle in a potential well. Assuming particles to be vortices<sup>23</sup> with mass  $M_V = \Phi_0^2 C / 2S$  tunneling through barriers of  $E_b = \gamma(f)E_J$ , one can estimate  $R_{00}$  from the analogy with single junctions<sup>52</sup> (moderate damping regime):

$$R_{00} \approx 7.2 R_{qf} \sqrt{120 \pi s} e^{-s}, \quad (2)$$

where  $s$  is given by

$$s = \frac{7.2}{\hbar} \sqrt{2 E_b M_V} \left( 1 + \frac{0.87}{\sqrt{\beta_{c,v}}} \right). \quad (3)$$

$\beta_{c,v} = 2\gamma\beta_c$  is the vortex McCumber parameter. We have fitted our data to Eq. (2) and in Table III, the measured values of  $s$  are given as  $s_{\text{meas}}$ .

In Table III we have listed the values of the tunnel rates calculated from Eq. (3) as  $s_{\text{sv}}$ . We used the quasistatically calculated, classical mass  $M_V$  for a vortex, the measured barrier height and an effective damping of the normal-state resistance. We find that the measured tunnel rates are lower than expected. As shown in Table III, the measured values of  $s$  are about a factor of 4 higher than the ones calculated in the simple approximation. This increase by a factor of 4 is consistent with the single vortex model when using a mass that is an order of magnitude higher than the one calculated in the quasistatic approximation. One may expect large de-

viations from the statically calculated mass in the dynamical situation if a vortex is not moving as a rigid object.

In the model discussed above, vortices in the array tunnel from cell to cell. Alternatively, single vortices can also cross the whole array width at once. The same model as above applies, but  $R_{00}$  in Eq. (2) is a factor  $N$  larger. This would make the discrepancy between model and experiment a factor of 8 instead of 4.

Another possible model for quantum tunneling of vortices that includes collective effects but also disorder, is variable-range hopping as discussed by Fisher *et al.*<sup>53</sup> In this model the vortex-hopping length increases with decreasing temperature. As the hopping length becomes larger than the distance between vortices the temperature dependence changes from the classical Arrhenius behavior to a power law of the form  $\exp-(T_0/T)^r$ , where  $T_0$  is a function of the barrier height and  $r$  is a constant between 2/3 and 4/5. In this model a temperature-independent resistance arises at low temperatures when the vortex hopping length equals the width of the finite sample (60 cells in our case). We have fitted the resistance in the temperature-dependent regime to the predicted Arrhenius behavior at high temperatures and the predicted power law at lower temperatures. For most arrays this does not improve the agreement. In view of the large number of fitting parameters involved we do not want to draw definite conclusions about the validity of this model.

## VII. CONCLUSION

We have reported on measurements of quantum phase transitions in Josephson-junction arrays at zero and nonzero magnetic field. S–I transitions have been studied as a function of the  $E_C/E_J$  ratio and as a function of the applied magnetic field. For the S–I transitions as a function of

$E_C/E_J$ , we find qualitatively similar behavior for zero and commensurate values of the applied field. Measurements indicate a superconductor–insulator transition at the lowest temperatures with a magnetic-field-dependent critical resistance [ $R_0^*(f)$ ] and critical  $E_C/E_J$  ratio [ $x_{cr}(f)$ ].

When quantum fluctuations are large already in zero field (arrays with  $E_C \approx E_J$ ), an applied magnetic field can drive a superconducting array into the insulating regime. This magnetic-field-tuned S–I transition arises from a collective Bose-condensation of vortices and critical exponents of the transitions near zero field are in good agreement with theoretical expectations. Field-tuned transitions also occur near fractional values of  $f$  with similar critical behavior.

From simple considerations, the influence of quantum phase fluctuations on the vortex dynamics is a lowering of the cell-to-cell barrier, the depinning current, and the vortex mass. The trends that we observe in our arrays close to the S–I transition are in agreement with this picture. Quantitatively, there are deviations from theoretical models indicating that the vortex dynamics near the transition is still not

completely understood. A similar conclusion can be drawn for the dual experiments at the insulating side of the S–I transition where  $2e$ -charge excitations dominate dynamics. Because junction parameters are so well known, it should be possible to gain a more quantitative understanding of quantum dynamics near the S–I transition. Studies should consider the discreteness of the lattice, random offset charges, the coupling to quasiparticles, and possibly edge effects. If these effects can be incorporated, experiments on Josephson-junction arrays could quantitatively test the validity of theoretical models describing two-dimensional systems of interacting bosons.

## ACKNOWLEDGMENTS

We thank R. Fazio, M. P. A. Fisher, J. V. José, G. Schön, and A. van Otterlo for valuable discussions. This work was in part supported by the Dutch Foundation for Fundamental Research on Matter (FOM).

- 
- <sup>1</sup>J. E. Mooij and G. Schön, in *Single Charge Tunneling*, edited by H. Grabert and M. H. Devoret (Plenum, New York, 1992), Chap. 8, and references therein.
- <sup>2</sup>Y. Liu and A. M. Goldman, *Mod. Phys. Lett. B* **8**, 277 (1993), and references therein.
- <sup>3</sup>S. Katsumoto, *J. Low Temp. Phys.* **98**, 287 (1995), and references therein.
- <sup>4</sup>W. J. Elion, J. J. Wachters, L. L. Sohn, and J. E. Mooij, *Phys. Rev. Lett.* **71**, 2311 (1993).
- <sup>5</sup>Yu. V. Nazarov and A. A. Odintsov, *Physica B* **194–196**, 1737 (1994); A. A. Odintsov and Yu. V. Nazarov, *Phys. Rev. B* **51**, 1133 (1995); M. Y. Choi, *ibid.* **50**, 10 088 (1994); *Ady Stern, Phys. Rev. B* **50**, 10 092 (1994).
- <sup>6</sup>L. J. Geerligs, M. Peters, L. E. M. de Groot, A. Verbruggen, and J. E. Mooij, *Phys. Rev. Lett.* **63**, 326 (1989).
- <sup>7</sup>H. S. J. van der Zant, L. J. Geerligs, and J. E. Mooij, *Europhysics Lett.* **19**, 541 (1992).
- <sup>8</sup>C. D. Chen, P. Delsing, D. B. Haviland, and T. Claeson, *Phys. Scr. T* **42**, 182 (1992).
- <sup>9</sup>R. S. Fishman and D. Stroud, *Phys. Rev. B* **35**, 1676 (1987).
- <sup>10</sup>H. S. J. van der Zant, F. C. Fritschy, W. J. Elion, L. J. Geerligs, and J. E. Mooij, *Phys. Rev. Lett.* **69**, 2971 (1992).
- <sup>11</sup>C. D. Chen, P. Delsing, D. B. Haviland, Y. Harada, and T. Claeson, *Phys. Rev. B* **51**, 15 645 (1995).
- <sup>12</sup>M. P. A. Fisher, *Phys. Rev. Lett.* **65**, 923 (1990).
- <sup>13</sup>M. P. A. Fisher, G. Grinstein, and S. M. Girvin, *Phys. Rev. Lett.* **64**, 587 (1990).
- <sup>14</sup>R. Fazio and G. Schön, *Phys. Rev. B* **43**, 5307 (1991).
- <sup>15</sup>B. J. van Wees, *Phys. Rev. B* **44**, 2264 (1991).
- <sup>16</sup>R. Fazio, A. van Otterlo, G. Schön, H. S. J. van der Zant, and J. E. Mooij, *Helv. Phys. Acta* **65**, 228 (1992).
- <sup>17</sup>T. S. Tighe, M. T. Tuominen, J. M. Hergenrother, and M. Tinkham, *Phys. Rev. B* **47**, 1145 (1993).
- <sup>18</sup>P. Delsing, C. D. Chen, D. B. Haviland, Y. Harada, and T. Claeson, *Phys. Rev. B* **50**, 3959 (1994).
- <sup>19</sup>A. Kanda, S. Katsumoto, and S. Kobayashi, *J. Phys. Soc. Jpn.* **63**, 4306 (1994); A. Kanda and S. Kobayashi, *J. Phys. Soc. Jpn.* **64**, 19 (1995).
- <sup>20</sup>A. van Otterlo, K-H Wagenblast, R. Fazio, and G. Schön, *Phys. Rev. B* **48**, 3316 (1993).
- <sup>21</sup>H. S. J. van der Zant, H. A. Rijken, and J. E. Mooij, *J. Low Temp. Phys.* **79**, 289 (1990).
- <sup>22</sup>T. P. Orlando, J. E. Mooij, and H. S. J. van der Zant, *Phys. Rev. B* **43**, 10 218 (1991).
- <sup>23</sup>H. S. J. van der Zant, F. C. Fritschy, T. P. Orlando, and J. E. Mooij, *Phys. Rev. Lett.* **66**, 2531 (1991).
- <sup>24</sup>H. S. J. van der Zant, F. C. Fritschy, T. P. Orlando, and J. E. Mooij, *Phys. Rev. B* **47**, 295 (1993).
- <sup>25</sup>S. Teitel and C. Jayaprakash, *Phys. Rev. Lett.* **51**, 1991 (1983); *Phys. Rev. B* **27**, 598 (1983).
- <sup>26</sup>T. C. Halsey, *J. Phys. C* **18**, 2437 (1985).
- <sup>27</sup>W. Y. Shih and D. Stroud, *Phys. Rev. B* **30**, 6774 (1984).
- <sup>28</sup>R. Théron, S. E. Korshunov, J. B. Simond, Ch. Leemann, and P. Martinoli, *Phys. Rev. Lett.* **72**, 562 (1994).
- <sup>29</sup>L. J. Geerligs, in *Physics of Nanostructures*, Proceedings of the 38th Scottish University Summer School in Physics, edited by J. H. Davis and A. R. Long (IOP, Bristol, 1992), p. 171.
- <sup>30</sup>U. Geigenmüller and G. Schön, *Europhys. Lett.* **10**, 765 (1989).
- <sup>31</sup>V. Ambegaokar and A. Baratoff, *Phys. Rev. Lett.* **10**, 846 (1963).
- <sup>32</sup>V. L. Berezinskii, *Zh. Eksp. Teor. Fiz.* **59**, 907 (1970) [*Sov. Phys. JETP* **32**, 493 (1971)]; J. M. Kosterlitz and D. J. Thouless, *J. Phys. C* **6**, 1181 (1973).
- <sup>33</sup>J. E. Mooij, B. J. van Wees, L. J. Geerligs, M. Peters, R. Fazio, and G. Schön, *Phys. Rev. Lett.* **65**, 645 (1990).
- <sup>34</sup>M. Sugahara, *Jpn. J. Appl. Phys.* **24**, 674, (1985).
- <sup>35</sup>H. S. J. van der Zant and J. R. Phillips (unpublished). This is the same problem as the calculation of the field distribution of a single vortex in an array where self-fields are important [see J. R. Philips, H. S. J. van der Zant, J. White, and T. P. Orlando, *Phys. Rev. B* **47**, 5219 (1993)]. When only self-inductances are included the penetration depth is  $\lambda_J$  which is proportional to  $1/\sqrt{I_c}$ . When the inductive coupling between all cells is included the penetration depth is  $\lambda_{\perp}$ , which is proportional to  $1/I_c$ .

- <sup>36</sup>G. Luciano, U. Eckern, and J. G. Kissner, *Europhys. Lett.* **32**, 669 (1995).
- <sup>37</sup>J. G. Kissner and U. Eckern, *Z. Phys. B* **91**, 155 (1993).
- <sup>38</sup>R. Fazio, A. van Otterlo, and G. Schön, *Europhys. Lett.* **25**, 453 (1994).
- <sup>39</sup>J. V. José and C. Rojas, *Physica B* **203**, 481 (1994); C. Rojas and J. V. José (unpublished).
- <sup>40</sup>M. Cha, M. P. A. Fischer, S. M. Girvin, M. Wallin, and A. P. Young, *Phys. Rev. B* **44**, 6883 (1991).
- <sup>41</sup>E. Granato and J. M. Kosterlitz, *Phys. Rev. Lett.* **65**, 1267 (1990).
- <sup>42</sup>Min-Chul Cha and S. M. Girvin, *Phys. Rev. B* **49**, 9794 (1994).
- <sup>43</sup>M. P. A. Fisher, *Phys. Rev. Lett.* **57**, 885 (1986).
- <sup>44</sup>M. V. Simkin, *Phys. Rev. B* **44**, 7074 (1991).
- <sup>45</sup>L. Jacobs, J. V. José, M. A. Novotny, and A. M. Goldman, *Phys. Rev. B* **38**, 4562 (1988).
- <sup>46</sup>A. D. Zaikin, in *Quantum Fluctuations in Mesoscopic and Macroscopic Systems*, edited by H. A. Cerdeira *et al.* (World Scientific, Singapore, 1991), p. 255.
- <sup>47</sup>A. F. Hebard and M. A. Paalanen, *Phys. Rev. Lett.* **65**, 927 (1990).
- <sup>48</sup>G. T. Seidler, T. F. Rosenbaum, and B. W. Veal, *Phys. Rev. B* **45**, 10 162 (1992); S. Tanda, S. Ohzeki, and T. Nakayama, *Phys. Rev. Lett.* **69**, 530 (1992).
- <sup>49</sup>In our original paper (Ref. 10), we had erroneously listed the value  $1/z_B$ .
- <sup>50</sup>W. W. Wu and P. W. Adams, *Phys. Rev. B* **50**, 13 065 (1994).
- <sup>51</sup>D. V. Averin, A. B. Zorin, and K. K. Likharev, *Zh. Eksp. Teor. Fiz.* **88**, 692 (1985) [*Sov. Phys. JETP* **61**, 407 (1985)]; U. Geigenmüller and G. Schön, *Physica B* **152**, 186 (1988); A. D. Zaikin and I. N. Kosarev, *Phys. Lett. A* **131**, 125 (1988).
- <sup>52</sup>J. M. Martinis, M. H. Devoret, and J. Clarke, *Phys. Rev. B* **35**, 4682 (1987).
- <sup>53</sup>M. P. A. Fisher, T. A. Tokayasu, and A. P. Young, *Phys. Rev. Lett.* **66**, 2931 (1991).